SLAC-PUB-16812

EVALUATING BEAM-LOSS DETECTORS FOR LCLS-2*

Alan S. Fisher#, Clive Field, Ludovic Nicolas, SLAC, Menlo Park, California 94025, USA

Abstract

The LCLS x-ray FEL occupies the third km of the 3-km SLAC linac, which accelerates electrons in copper cavities pulsed at 120 Hz. For LCLS-2, the first km of linac will be replaced with superconducting cavities driven by continuous RF at 1300 MHz. The normal-conducting photocathode gun will also use continuous RF, at 186 MHz. The laser pulse rate will be variable up to 1 MHz. With a maximum beam power of 250 kW initially, and eventually 1.2 MW, the control of beam loss is critical for machine and personnel safety, especially since losses can continue indefinitely in linacs, and dark current emitted in the gun or cavities can be lost at any time. SLAC protection systems now depend on ionization chambers, both local devices at expected loss sites and long gas-dielectric coaxial cables for distributed coverage. However, their ion collection time is over 1 ms, far slower than the beam repetition rate. We present simulations showing that with persistent losses, the space charge of accumulated ions can null the electric field inside the detector, blinding it to an increase in loss. We also report on tests comparing these detectors to faster alternatives.

INTRODUCTION

LCLS and LCLS-2

The Linac Coherent Light Source (LCLS) is an x-ray free-electron laser (FEL) that began operation in 2009 [1]. It occupies the third kilometer of SLAC's 3-km copper room-temperature linac. Both the linac and the photocathode radio-frequency (RF) gun are pulsed at 120 Hz with 2856 MHz. The first km of the linac was removed in the past year to make way for LCLS-2, which will use continuous 1300-MHz RF in superconducting cavities, with a normal-conducting photocathode RF gun at 186 MHz and a bunch rate of up to 1 MHz. Operation will begin (before upgrades) at an electron energy of 4 GeV and a beam power of 250 kW, increasing to 1.2 MW. Table 1 compares the parameters of both machines.

Beam Loss and Safety Systems

Beam-loss instrumentation follows a tiered structure. During normal operation, diagnostics monitor and locate sources of loss, and aid in tuning. The machine protection system (MPS) blocks the beam or halts it if losses exceed a threshold, or for other causes (insertion of an obstacle such as a valve, an excessive temperature). Beam containment (BCS) stops the accelerator if a loss of beam current or radiation from beam loss would indicate possible harm to people or to devices like protection collimators. Safety-systems detectors are deployed in twos for redundancy.

Table 1: Parameters of the LCLS normal-conducting linac and the LCLS-2 superconducting linac.

Parameter	**LCLS**	**LCLS-2**
Electron energy	15 GeV	4 (later 8) GeV
Bunch charge	20 to 250 pC	20 to 250 pC
Beam power	450 W	**0.25 (later 1.2) MW**
Gun frequency	2856 MHz	185.7 MHz
Linac frequency	2856 MHz	1300 MHz
RF pulse rate	120 Hz	Continuous
e^- bunch rate	120 Hz	92.9 (later 929) kHz
Photon energy	0.2 to 5 keV	1 to 15 (later 25) keV

The detectors discussed here are evaluated primarily for BCS, but their signals will be split outside the tunnel for independent processing for BCS, MPS, and diagnostics.

The highest level of protection, the personnel protection system (PPS), interlocks access to the machine and shuts it off if radiation is found in occupied areas. PPS instrumentation will not be further considered here.

Unlike LCLS, which has 8 ms (a 120-Hz period) to shut off, LCLS-2 has continuous RF. Losses must be detected in as little as 100 μs, after which the beam must be shut off within 100 μs (see Table 2). Losses can arise from high-power photocurrent, or from dark current due to field emission in the gun or linac modules. Dark current can be emitted at any time and can travel through several cryomodules in either direction depending on the RF phase at emission.

IONIZATION DETECTORS

BCS at SLAC has long relied on two types of ionization detector. We describe these here and discuss whether ion collection is sufficiently fast for LCLS-2.

Protection Ion Chamber (PIC)

A PIC is a point loss detector, placed within 0.5 m of a site such as a collimator needing protection against damage. Figure 1 shows the design, a stainless-steel cylinder containing a stack of 32 plates biased alternately at ground or (typically) −300 V. At this voltage, collection of electrons takes 2 μs, but ions require 1 ms.

Both the PICS and the LIONs discussed next are generally filled to 125 to 150 kPa with a mixture of 95% Ar and 5% CO_2. However, the LCSL-2 model and the experiment (both discussed below) use 100% Ar.

Long Ionization Chamber (LION)

A SLAC LION (Figure 2) is a gas-dielectric Heliax coaxial cable (made with continuous helically-wound copper strips) that detects losses along (typically) 30 to 50

*SLAC is supported by the U.S. Department of Energy, Office of Science, under contract DE-AC02-76SF00515
#afisher@slac.stanford.edu

Table 2: BCS requirements for point and line radiation detectors.

Device	Trip Level	Response Time
Point detector: Protects stoppers and collimators	Detect loss of 25 J in 100 ms, then shut off within 100 μs. Sample at least every 25 μs.	250 kW for 100 μs 25 kW for 1 ms 2.5 kW for 10 ms ≤250 W is safe
Long detector: Measure inside shielding wall for protection outside	Linac: 10 krad/hr over 10 m Beam Transfer Hall: 3–20 rad/hr (adjustable) over 5 m (lower due to less shielding)	600 ms

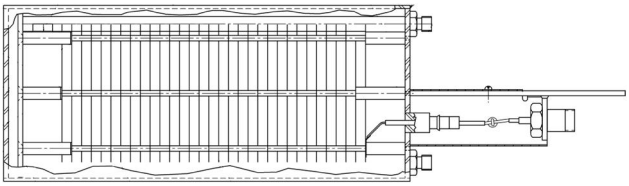

Figure 1: Cutaway view of a PIC. The housing is a stainless-steel cylinder with a 114-mm outer diameter and a 270-mm length. The 32 plates each have an area of 56.5 cm^2 and are 6.35 mm apart. The plates are alternately grounded or connected to a bias voltage.

m of the tunnel. A +250-V bias on the center conductor drives charge radially, with a collection time of 6 μs for electrons but 6 ms for ions. The charge moves in both directions along the cable. One end leads to a high-voltage supply, an integrator and a digitizer. The other end has a high-impedance termination drawing a small DC current, which indicates that the system is functioning.

1-D Model of an Ionization Chamber

The possible loss of significant beam power and an ion collection time far longer than the interval between pulses both suggest that ion space charge may accumulate inside a chamber. An experimental and numerical study of ionization chambers for protons in the NuMI experiment at Fermilab [2] found that ion screening can completely null the field in part of the chamber, creating a "dead zone." This motivated the development of a one-dimensional model of charge flow in the SLAC chambers.

The model assumes a uniform ionization rate $I(t)$ per unit volume generated by beam loss and a recombination rate per unit volume $\beta n_i n_e$ proportional to the product of electron and ion densities. The PIC behavior is computed for the x coordinate between a pair of plates. The signal current is then scaled by 31 to account for all plates. The LION model computes the radial behavior in a uniformly ionized 1-cm length of cable.

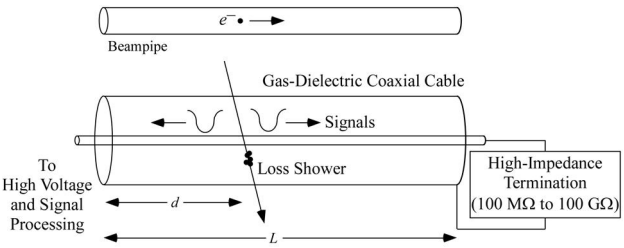

Figure 2: Sketch of LION. The normal inner- and outer-conductor diameters are18.1 and 46.5 mm respectively.

Both detectors are filled with 100 kPa of Ar, a common gas for ionization chambers, to avoid both the complexity of molecular fragmentation and also the creation of negative ions, which move as slowly as positive ions and would further contribute to the accumulation of space charge.

At this pressure, the mean free path is much smaller than the chamber size, and so particle drift is modeled by a mobility $\mu_{i,e}$ (with a velocity **v** proportional to the electric field **E**), although the electron mobility has a weak dependence on E. The particle flux $\mathbf{J}_{i,e}$ also includes a diffusive component. **E** is given self-consistently by Gauss's Law. The governing equations are:

$$\begin{aligned} \mathbf{J}_{i,e} &= \pm\mu_{i,e} n_{i,e}\mathbf{E} - D_{i,e}\nabla n_{i,e} \\ \frac{\partial n_{i,e}}{\partial t} &= -\nabla\cdot\mathbf{J}_{i,e} + I - \beta n_i n_e \\ \varepsilon_0\nabla\cdot\mathbf{E} &= e(n_i - n_e) \end{aligned} \tag{1}$$

Electrodes are charge sinks but not sources: electrons or ions can flow in but not out. The surface charge Q on each electrode is determined self-consistently through Gauss's Law and by the requirement that the bias supply provides enough charge to maintain a constant voltage:

$$\begin{aligned} Q &= \varepsilon\int_S \mathbf{E}\cdot d\mathbf{S} \\ V_0 &= -\int_a^b \mathbf{E}\cdot d\mathbf{u} \end{aligned} \tag{2}$$

We measure instead the charge Q_{ext} flowing through the external circuit from the bias supply. A change ΔQ is the sum of Q_{ext} and the charge of collected electrons or ions:

$$\Delta Q = Q_{\text{ext}} \pm e\int_S \mathbf{J}_{i,e}\cdot d\mathbf{S} \tag{3}$$

Radiation Field

A FLUKA model [3] relates the power lost on a beam stop to the radiation dose rate in the vicinity. From Figure 3, the dose rate at a radial distance of 50 cm is about 50 rad/(W·hr) over a longitudinal span of 50 cm.

Table 2 sets limits for long detectors of 3 to 20 rad/hr in the beam-transfer hall (between the linac and undulators) and 10 krad/hr in the linac. The corresponding power is 60 to 400 mW (36 to 240 mJ in the specified 600 ms), and 200 W (120 J in 600 ms) respectively. These powers are

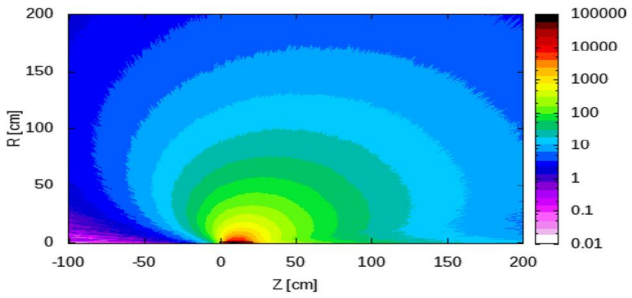

Figure 3: Model of the radiation field showing a loss near a beam stop. The color scale is in rad/(W·hr).

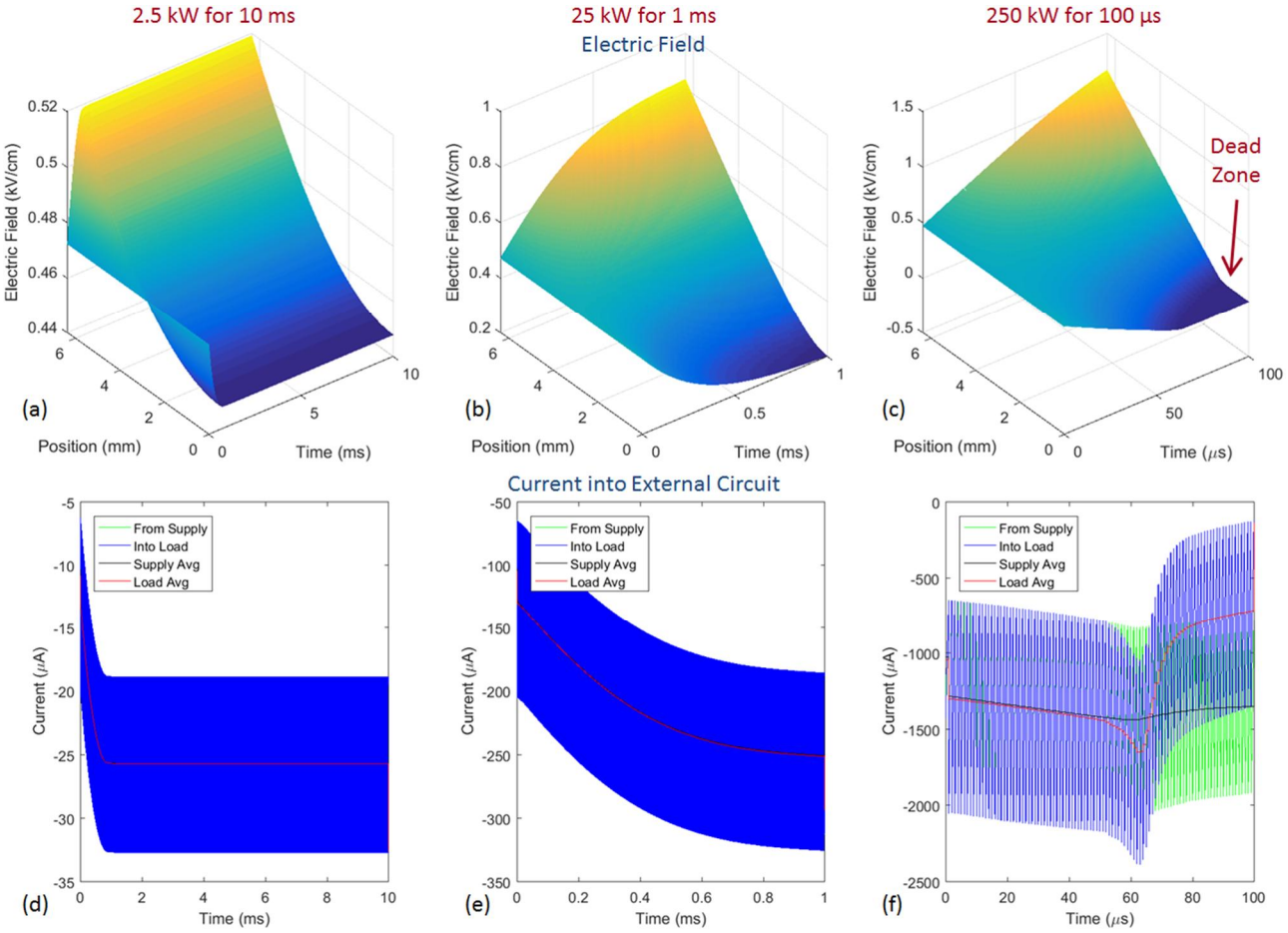

Figure 4: PIC model for three cases from Table 2. The electric field (a-c) progresses toward dead-zone formation as losses increase. In (c) the field near the positive electrode reaches zero after 60 µs. The external current equilibrates in 1 ms (d,e), but has a sudden reduction as the dead zone forms (f). The 1-MHz cycle of electron response is visible at the 100-µs time scale of (f) but becomes a broad blue band (covering an identical green band) in (d) and (e).

below the limits for point detectors, since the two types serve different purposes. The long detectors may trip first if placed near point losses.

Model Results: PIC

Figure 4 shows the evolution of the electric field (a–c) and the external current (d–f) in a PIC biased at −300 V, for three cases from Table 2. Losses with power levels of 2.5, 25 and 250 kW begin at $t = 0$, repeating at 1 MHz and reaching the 25-J trip threshold in 10, 1 and 0.1 ms respectively. When losses are low (a,d), the electric field between the plates is barely perturbed, but the current to the load takes 1 ms to equilibrate due to the slow ion drift. In the 250-kW case (c,f), field lines from the negative plate terminate on ion space charge before reaching the positive plate, completely screening the field there within 60 µs. Electron and ion transport halts in this dead zone (except for diffusion), and the density grows quickly with the periodic losses. The signal current becomes erratic.

Model Results: LION

In Figure 5 a LION biased at the standard +250 V exhibits similar behavior, exacerbated by the longer electrode separation and somewhat lower voltage. A negative bias would be worse: the field's $1/r$ dependence makes it weaker at the outer electrode and so easier to screen.

Because the trip levels of Table 2 for long detectors (≤200 W) are much lower than those for point detectors and below the moderate loss of Figure 5(a), a dead zone does not develop. But if the LION is exposed to a large point loss not protected by a point detector, then it can develop a dead zone.

ALTERNATIVE DETECTORS

The slow ion response compared to the bunch separation and the required trip time, along with the formation of a field-free dead zone for a loss of the full beam power (even before the upgrade to 1.2 MW), led us to consider alternatives not based on gas ionization.

For point losses we are evaluating diamond detectors [4]. Losses generate electron-hole pairs in a 1-cm^2 slice of synthetic polycrystalline diamond. The high mobility in a thin (500 µm) crystal gives 5-ns pulses.

For long detectors we are considering Cherenkov emission in radiation-hard optical fibers. A multimode fiber with a 600-µm core [5] was tested for radiation hardness up to 1.25 Grad for use in the LHC at CERN, in

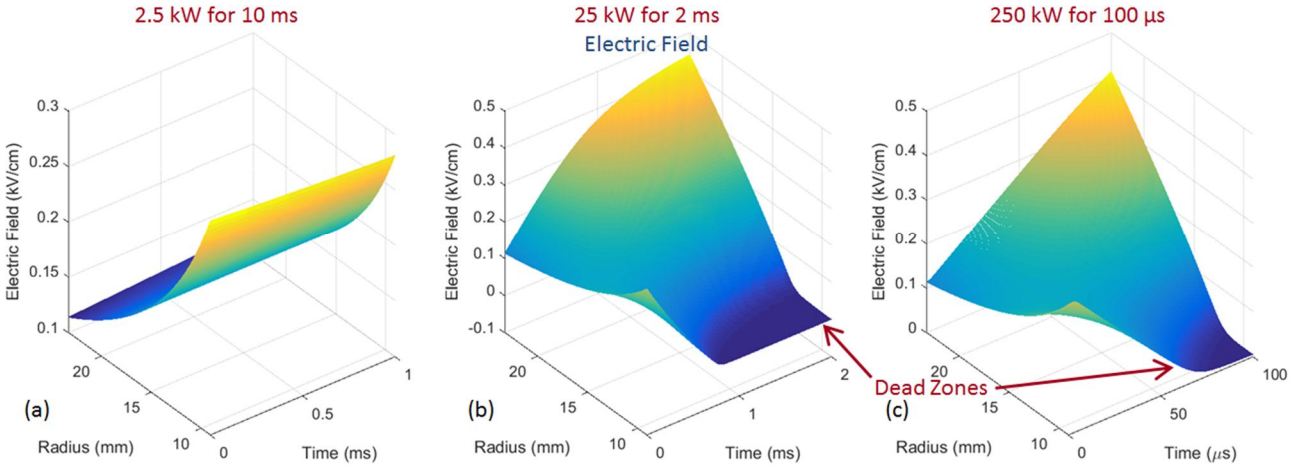

Figure 5: LION model for the cases of Figure 4. Due to the longer drift distance, the dead zone appears for a lower loss.

particular in the CMS end cap [6–8]. These would be installed in one-sector (100 m) lengths. A photomultiplier (PMT) or silicon photomultiplier (SiPM) would detect the light at one end; at the other, an LED outside the tunnel would periodically pulse to monitor transmission.

EXPERIMENTAL TEST

An experimental test compared a PIC and a short LION to two types of diamond (standard and high-radiation) and to an optical fiber run along the LION (Figure 6). A 180-pC, 5.115-GeV electron beam hit tungsten plates at 5 Hz. The diamonds and fiber were faster and less noisy than the PIC and LION. We next will test 100 m of fiber and diamonds in a linac sector to gain operational experience.

REFERENCES

[1] P. Emma *et al.*, "First lasing and operation of an ångstrom-wavelength free-electron laser," Nature Photonics **4** (2010) 641.

[2] R.M. Zwaska *et al.*, "Beam Tests of Ionization Chambers for the NuMI Neutrino Beam," IEEE Trans Nucl. Sci. **50** (2003) 1129.

[3] M. Santana Leitner, "Fluence to dose conversion E-curves for silicon and polyethylene. A FLUKA user-routine to convert fluence into energy deposition in small radiation sensitive accelerator components," SLAC Radiation Physics Note RP-14-20, example 3, doses near a stopper.

[4] https://cividec.at/

[5] FBP600660710, Polymicro division of Molex.

[6] I. Dumanoglu *et al.*, "Radiation-hardness studies of high OH^- content quartz fibres irradiated with 500 MeV electrons," Nucl. Instrum. Methods A **490** (2002) 444.

[7] K. Cankoçak *et al.*, "Radiation-hardness measurements of high OH^- content quartz fibres irradiated with 24 GeV protons up to 1.25 Grad," Nucl. Instrum. Methods A **585** (2008) 20.

[8] F. Duru *et al.*, "CMS Hadronic EndCap Calorimeter Upgrade Studies for SLHC 'Čerenkov Light Collection From Quartz Plates'," IEEE Trans Nucl. Sci. **55** (2008) 734.

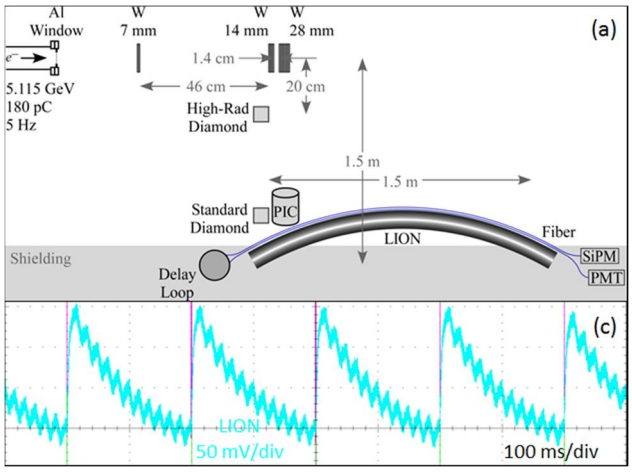

Figure 6: (a) Experimental layout. Signals from (b) PIC and diamonds; (c) LION, with a very slow time scale and large 60-Hz noise; (d) PMT and SiPM. (The SiPM pulse is long because a transimpedance amplifier is needed.)